PROCEEDINGS OF SPIE

SPIEDigitalLibrary.org/conference-proceedings-of-spie

Design and characterization of MECSELs for widely tunable (>25 THz) continuous wave operation

Patrik Rajala, Philipp Tatar-Mathes, Hoy-My Phung, Jesse Koskinen, Sanna Ranta, et al.

Patrik Rajala, Philipp Tatar-Mathes, Hoy-My Phung, Jesse Koskinen, Sanna Ranta, Mircea Guina, Hermann Kahle, "Design and characterization of MECSELs for widely tunable (>25 THz) continuous wave operation," Proc. SPIE 11984, Vertical External Cavity Surface Emitting Lasers (VECSELs) XI, 1198404 (4 March 2022); doi: 10.1117/12.2610649

SPIE.

Event: SPIE LASE, 2022, San Francisco, California, United States

Best Student Paper Award

Design and characterization of MECSELs for widely tunable (> 25 THz) continuous wave operation

Patrik Rajala *, Philipp Tatar-Mathes, Hoy-My Phung, Jesse Koskinen, Sanna Ranta, Mircea Guina, and Hermann Kahle

Optoelectronics Research Centre (ORC), Physics Unit / Photonics, Faculty of Engineering and Natural Sciences, Tampere University, Korkeakoulunkatu 3, 33720 Tampere, Finland

ABSTRACT

Membrane external-cavity surface-emitting lasers (MECSELs) are vertically emitting semiconductor lasers that combine all the benefits of VECSELs (vertical-external-cavity surface-emitting lasers) with the new degree of freedom in creating gain structures without monolithically integrated distributed Bragg reflectors (DBRs). The absence of the DBR and the substrate, and the use of a very thin gain membrane (typically some hundreds of nanometers), which can be sandwiched between two transparent heat spreaders, represents the best solution for heat removal. The membrane configuration also allows the option of double side pumping, which in turn makes it possible to utilize an extensive amount of quantum well (QW) groups as well as multiple kinds of QWs in a periodic laser gain structure. Here we report on design strategy and results of different kinds of approaches on broadband, relatively high power MECSEL gain structures. Especially efficient pump absorption, sufficient gain on several different wavelengths and carrier mobility during laser operation, are discussed. We also present the characteristics of the laser systems created. Results show ∼83 nm (∼25 THz) tuning range with more than 100 mW of power at all wavelengths at room temperature operation. Strategies for further development are discussed as well.

Keywords: laser, MECSEL, membrane laser, semiconductor, VECSEL, power-scaling, thermal management, broadband gain, tunable lasers

1. INTRODUCTION

Tunability of semiconductor lasers has been of high interest for about 20 years now.[1] Possible applications range from optical telecommunication systems to broadband sensors,[2,3] and from atomic physics[4] to spectroscopy.[5,6] In recent years, both vertical-external-cavity surface-emitting lasers (VECSELs[7,8]) and membrane external-cavity surface-emitting lasers (MECSELs[7–10]) as members of the vertically emitting semiconductor laser family, have been pushed to reach wider tuning ranges. Figure 1 shows these recent advances and how the work presented in this paper compares to them.

The wavelength range around 1 µm is of special interest, for example for spectroscopic[11] and pump-probing gain measurement applications that require both excellent beam properties, which MECSELs and VECSELs provide, and a wide tuning range. Another reason to work in this wavelength range is that the material system utilized is well-known, which allows strict focusing on research on the design possibilities regarding wavelength tunability of MECSELs.

Many of the advancements in VECSEL's tuning range were realized through adding complexity to the final device, such as through multi chip cavity configuration[12] or through careful gain element reflectance engineering,[13] or have been achieved in longer wavelength ranges and with other material systems.[14]

In the present paper, we explore the tuning possibilities of MECSELs. In MECSELs, an optically-pumped multi-quantum-well containing semiconductor membrane is sandwiched between two optically transparent heat spreaders and acts as gain element. Of particular interest is the MECSEL's greater freedom of active area design that is not limited by features of monolithically integrated distributed Bragg reflectors (DBRs), that for example VECSELs utilize. The DBR ultimately limits the laser's operating wavelength range, as it has a

*Further author information: Send correspondence to Patrik Rajala, E-mail: patrik.rajala@tuni.fi

Vertical External Cavity Surface Emitting Lasers (VECSELs) XI, edited by Mircea Guina, Proc. of SPIE Vol. 11984, 1198404 · © 2022 SPIE
0277-786X · doi: 10.1117/12.2610649

more limited stop band width compared to dielectric coatings of more complex architecture, and it possesses a relatively low thermal conductivity.[15–17] On the other hand, the MECSEL enables double-side pumping[18] (DSP), which allows a significantly more homogeneous pump power distribution inside the structure and, due to the double-side access, more QWs to be pumped. This in turn makes it possible to design and fabricate thicker active areas with more QWs and QW groups. Moreover, double-side cooling via the transparent heat spreaders is a built-in feature.

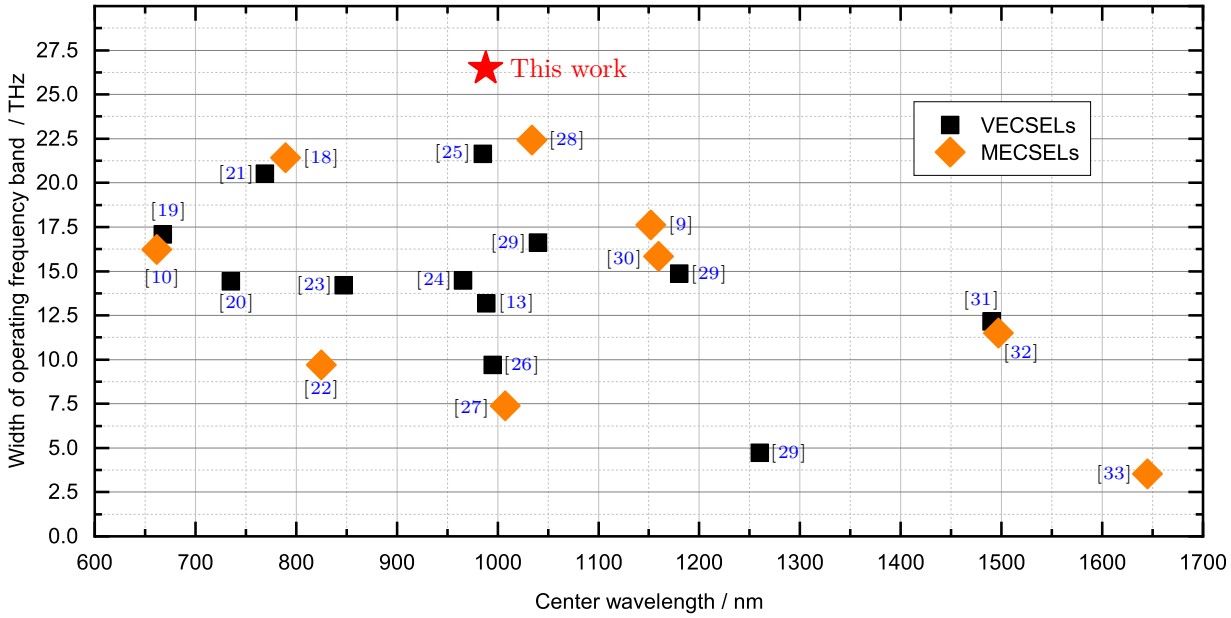

Figure 1. Overview over a selection of VECSELs (full black squares) with relatively wide tuning ranges, and MECSELs (full orange rhombuses) covering the major part of yet realized devices in terahertz, plotted over different emission wavelengths. Both, QW and QD (quantum dot) based laser active structures are included.

2. DESIGN AND PRE-CHARACTERIZATION OF WIDELY TUNABLE MECSELS

One of the advantages of MECSELs is its ease of fabrication and characterization, and in the case of widely tunable MECSELs, no significant complexity is added to these processes. The main novelty lies in the design as well as in the final device capabilities. The following subsections will give an overview regarding the main design and growth aspects of broadband MECSELs.

2.1 Design and structure simulation

To significantly extend the tuning range of a surface-emitting semiconductor laser with respect to the established standard, more than one kind of QW in the structure must be used. While it is known that using more QWs per QW group or widening the QW thickness can provide more tuning range due to the increase in available energy states, these solutions have significant limits on how much they can provide extra tuning range and in what kind of structures they can be employed in, e.g. because of extensive local strain. In the 1 µm wavelength range on which we focus in this paper, the number of QWs in a QW group can not be increased further beyond two, as local strain sums up and strain compensation layers must be introduced accordingly. Therefore, another strategy has to be employed.

In 2005, Leinonen *et al.*[34] demonstrated a VECSEL capable of operating on two different wavelengths at the same time, which proved that the operation of a surface-emitting laser utilizing two different kinds of QWs in a single structure is certainly feasible. There were two main design ideas in this dual-wavelength VECSEL: (1) separating the different kinds of QWs from each other with electron blocking layers (EBLs) to prevent most of the excited charge carriers from diffusing extensively towards the lowest energy states inside the structure, i.e. the

QWs of the longer emission wavelength, and (2) matching the standing wave of the electric field during operation in a way that ensures that when the laser is operated on the shorter wavelength, QWs corresponding to that emission wavelength are in the nodes of the electric field and the other QWs are in the antinodes, and vice versa for the longer wavelength operation. To move from dual-wavelength operation to continuous broadband tuning operation, but at a single wavelength at a time, design point (1) is still valid, as the charge carriers will otherwise always diffuse mostly towards the energy states of the longer wavelength QWs. This was nicely demonstrated by the photoluminescence (PL) measurement results in LEINONEN *et al.*[34] Point (2) is not as straightforward for the case of continuous tuning. It is clear that on the shorter wavelength end it is beneficial to have clear matching of antinodes on the shorter emission wavelength QWs and matching of nodes on the longer emission wavelength QWs to minimize the re-absorption by the long wavelength QWs during operation. However, the opposite way this should not play a role, as the QWs of shorter emission wavelength are not capable of absorbing photons emitted by the QWs of longer emission wavelength. Thus it is more important to just have a good matching of antinodes on the QWs of the longer emission wavelength, when we are operating on the longer side of the wavelength range.

In addition to the aspects mentioned, the choice of QW materials and the consideration of pump power distribution inside the structure during operation, are of high importance. For the choice of QW materials, we must consider the tunability of a single QW type. For VECSELs consisting of a single type of QW, a wide tuning range in this wavelength range has been demonstrated for example by BORGENTUN *et al.*[13,26] with 32 nm and 43 nm, respectively, and by BRODA *et al.*[25] with 70 nm (without temperature tuning). For MECSELs the latest record values were published by YANG *et al.*[9,28] and PRIANTE *et al.*[30] within the 1.0 µm to 1.2 µm range, and by KAHLE *et al.*[18] in the 780 nm range. These record values (see Fig. 1) were reached, although wide tuning was not intended and the semiconductor gain structures were not optimized for broadband emission, due to the MECSEL's intrinsic benefit[28] of not having a DBR close to the active region. However, as seen from these results, the tuning range is not evenly distributed around the center wavelength, but follows the typical inverted parabolic behaviour, which reassembles the spectral shape of the gain above laser threshold (if the cavity mirrors possess a flat reflection characteristic). Naturally, the choice of QW materials is a trade-off between maximum tuning range and constant emission power everywhere within, when using multiple QW types in a single structure. To receive a relatively flat emission power distribution throughout the tuning range, based on previous experiments, a separation of 60 nm in nominal emission wavelengths was chosen. This was achieved by using 7 nm thick InGaAs QWs with an In fraction of 13.0 % and 20.5 % respectively. GaAs barriers, GaAsP strain compensation layers, AlAs EBLs, and lattice matched GaInP window layers were used in the structure.

The pump power distribution during operation was taken into account when deciding the number and distribution of the chosen QWs inside the structure. QWs of the shorter emission wavelength (950 nm) have 37 % less quantum confinement for electrons and 33 % for holes compared to the 1010 nm QWs. Thus they provide significantly less gain. In order to have a (more) homogeneous emission characteristic throughout the tuning range, more of the short wavelength QWs must be utilized than of those of longer nominal emission wavelength. Based on own COMSOL® simulations, we were able to derive that ~ 2 µm is a good value of total thickness for the structure so that we are still able to pump all QWs sufficiently with single-side pumping (SSP)[35] under the given conditions. Even though the structure was designed to be double-side pumped, for comparison we wanted the structure to be able to operate with SSP as well for the purpose of investigating changes between the pumping regimes. Thus we decided to grow the 2 µm thick structure, which allows us to use eleven QW groups of two QWs per group, when we take into account how much spacer, barrier, charge carrier blocking, and strain compensation layers are also needed. To match the ~ 35 % difference in quantum confinement between the two types of QWs, a relation of seven short to four long wavelength QW packages was chosen.

Achieving a more homogeneous pump power distribution during DSP, the QW distribution was chosen to be symmetric when looking from the middle of the structure. Due to antinode and node matching the structure itself in detail is not completely symmetric as the placements and spacer layer thicknesses were adjusted last in the design process. This was done by simultaneously matching antinodes on QWs of the shorter wavelength and nodes on the QWs of the longer wavelength on the shorter target wavelength of 950 nm. The same was done for the antinodes on the QWs of the longer wavelength on the longer target wavelength of 1010 nm. Figures 2a and 2b show the simulated standing wave of the electric field intensity inside the structure during operation on wavelengths of 953 nm and 1009 nm, respectively. The structure was designed using the SimuLase® software and

the optical field simulations were made using the transfer matrix method in the expected lasing temperature of 350 K. In addition to the node and antinode matching described above, Figs. 2a and 2b show the ordering of the QW groups in five sections. This kind of order was chosen as a balance between keeping the structure simple

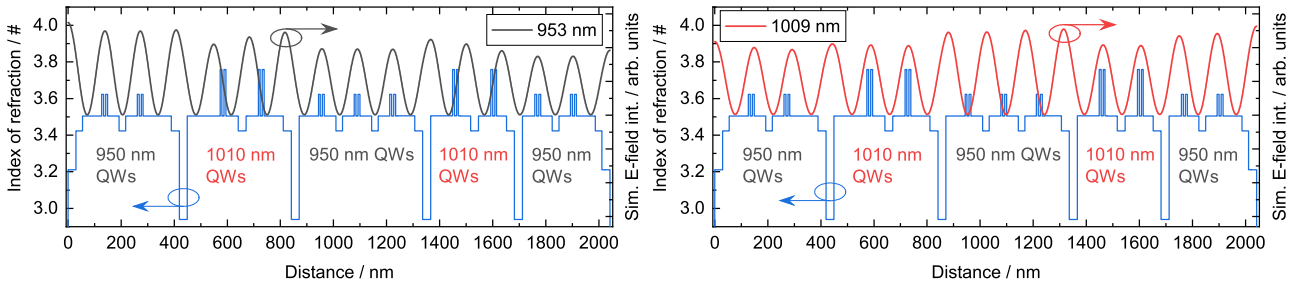

Figure 2. The gain membrane's architecture is shown. (a) Refractive index (blue solid line) and the simulated standing wave E-field intensity (solid dark grey line) of the short wavelength (nominally 950 nm) resonance are plotted over the thickness of the gain membrane. (b) Refractive index (blue solid line) and the simulated standing wave E-field intensity (solid red line) of the long wavelength (nominally 1010 nm) resonance are plotted over the thickness of the gain membrane.

enough to have good antinode and node matching on different wavelengths without thickening the structure needlessly as well as having a rather balanced amount of pump light reaching each of the QW group sections based on the COMSOL® calculations mentioned before. In addition to that EBLs had to be inserted. As a consequence of this trade-off, three antinodes (at distance ∼425 nm, 850 nm, and 1350 nm, see Figs. 2a and 2b) could not be brought in overlap with any QW pair as the space was needed for the EBLs.
The sample was mounted in the setup shown in Fig. 4 in the same orientation as it is depicted in Figs. 2a and 2b. Therefore, when applying SSP, a slight benefit for right side pumping is likely, as the barriers around the QWs are thicker on the left side of the structure. This might compensate the smaller pump power density on the left side of the gain membrane, when pumping from the right. A more homogeneous pumping condition for all QWs would be the consequence, which in turn would lead to better performance. See therefore the characterization results in Subsec. 3.4.
With the COMSOL® calculations we could estimate that 62 % of the pump light is absorbed in the shorter QW group sections and 33 % in the longer QW group sections. Considering the seven to four relation in the number of QWs, this is a very good balance in terms of QWs receiving an even amount of pump light, when finally applying DSP.

2.2 Photoluminescence characterization

The structure was grown by molecular beam epitaxy (MBE) with a VG V80 machine. While the growth parameters of all of the semiconductor materials used in this structure are known very well, the usage of more than one kind of QW in a single structure requires some uncommon calibration methods. The method of choice applied here was to first grow PL samples for each kind of QW separately, fine tune their material composition, and then combine them in the final structure. The PL calibration samples contain only one barrier and one QW group with two QWs of the same kind in it. Figure 3 shows the measured PL curves of both of the PL calibration samples as well as the final structure's PL curve. There we can see that the PL signal of the final structure is very much as expected based on the PL signals from the two separate QW calibration samples. The peak PL emission wavelengths are very close to what was desired, as we expect the gain maximum to be 15 to 25 nm red-shifted during laser operation. A much higher intensity of the PL signal of the final device was also expected, as there are a total of eleven QW groups compared to the one of the calibration samples. If we look at the calibration samples' PL intensity compared to each other, we can also see the aforementioned difference in quantum confinement, as the 1010 nm QWs emit an almost twice as strong PL signal. However, this effect has been quite well balanced with the QW distribution, as in the final device the relative difference between the PL signal from the two peak wavelengths is much smaller and actually the signal from the shorter wavelength

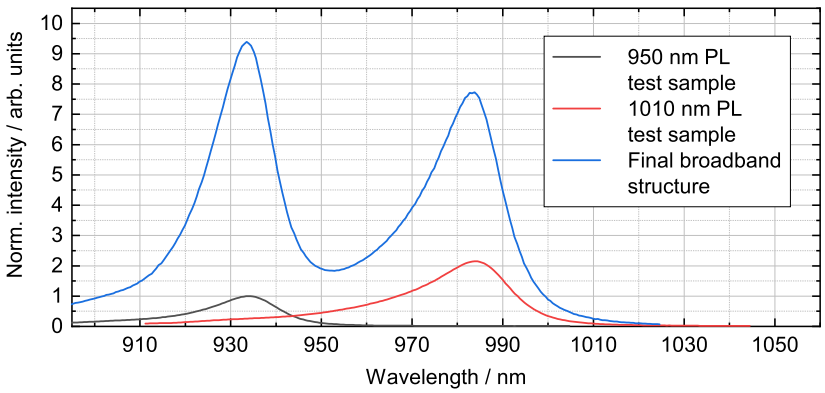

Figure 3. The PL signal at room temperature of the final broadband laser structure (blue) compared to the 950 nm QW calibration sample's (dark grey) and 1010 nm QW calibration sample's (red) PL. Measurement was done with a RPM 2000 system using a 785 nm continuous wave excitation laser. The intensities are normalized to the 950 nm QW calibration sample's intensity.

QWs is slightly better. This also leads us to believe that the EBLs are working as intended and prevent the longer wavelength QWs from attracting the vast majority of all charge carriers, if we compare this result to the PL results shown by Leinonen *et al.*[34].

3. LASER CHARACTERIZATION

In the following, the characterization setup, as well as the measurements performed in the same, are described in detail. All presented results in this section have been performed at the same heat sink temperature of 20°C. Also, the same laser cavity mirrors and the same cavity configuration have been used for all measurements.

3.1 Experimentation setup

A schematic illustration of the characterization setup is shown in Fig. 4. The V-cavity consisted of a plane outcoupling mirror M3 with a reflectivity of $R_{\mathrm{M3}} = (99.5 \pm 0.3)\,\%$, and two curved high-reflecting mirrors M1 and M2, which both had the same reflectivity of $R_{\mathrm{M1,\,M2}} > 99.9\,\%$ and the same radius of curvature of $r_{\mathrm{M1,\,M2}} = 300\,\mathrm{mm}$. The mirror distances of M1 and M2 to the gain membrane sandwich were adjusted to $L_1 = 291\,\mathrm{mm}$ and $L_2 = 293\,\mathrm{mm}$. M3 was positioned under an opening angle of 11° between L_2 and L_3. The distance between M2 and M3 was $L_3 = 291\,\mathrm{mm}$. For tuning a 1 mm thick birefringent filter was used, inserted in the L_3 cavity arm in an orientation to support parallel polarization. The calculated cavity mode diameter on the gain membrane was about 250 µm using the ray transfer method for a Gaussian TEM_{00} beam.

Two identical 808 nm LIMO diode lasers (only two construction numbers apart from each other) coupled into identical multi-mode fibers (MHP200L02 from THORLABS) with a 200 µm core diameter and a numerical aperture of 0.22 were used as a pump source. The fiber output was collimated by a $f = 100\,\mathrm{mm}$ anti reflection coated plano-convex lens, and focused onto a spot size of about 330 µm in diameter by a 90° off-axis parabolic mirror (MPD249H-M01 from THORLABS) with a protected gold reflection coating ($R_{808\,\mathrm{nm}} > 96\,\%$) and a reflected focal length of 101.6 mm. Thus, the ratio between the cavity and pump mode diameter was about 0.76, which is within the suggested optimum[36] from 0.65 to 0.82 derived by Laurain *et al.* via simulations. The parabolic mirror used in these experiments has a diameter of 50.8 mm as well as a hole with a diameter of 3 mm that does not cut the intra cavity laser mode. The collimated pump beam irradiated on the parabolic mirror covered almost the whole area of this mirror. For the pump beam, the losses caused by this 3 mm hole were investigated and were below 1 %, and therefore negligible. Nevertheless, the incident pump power P_{pump} was determined via measuring the power reflected by the parabolic mirror. Therefore, all reflection losses as well as the losses introduced by the centered 3-mm-through-hole were taken into account. With an angle of incidence of the pump laser, that ranges from almost 0° to less than 15°, this pump approach enables a nearly circular pump spot with $D_{\mathrm{p,\,sag}}/D_{\mathrm{p,\,tan}} > 0.96$ in the focus. The MECSEL gain membrane sandwiched between transparent heat spreaders (SiC in the present case), in the following called MECSEL gain element, was mounted between

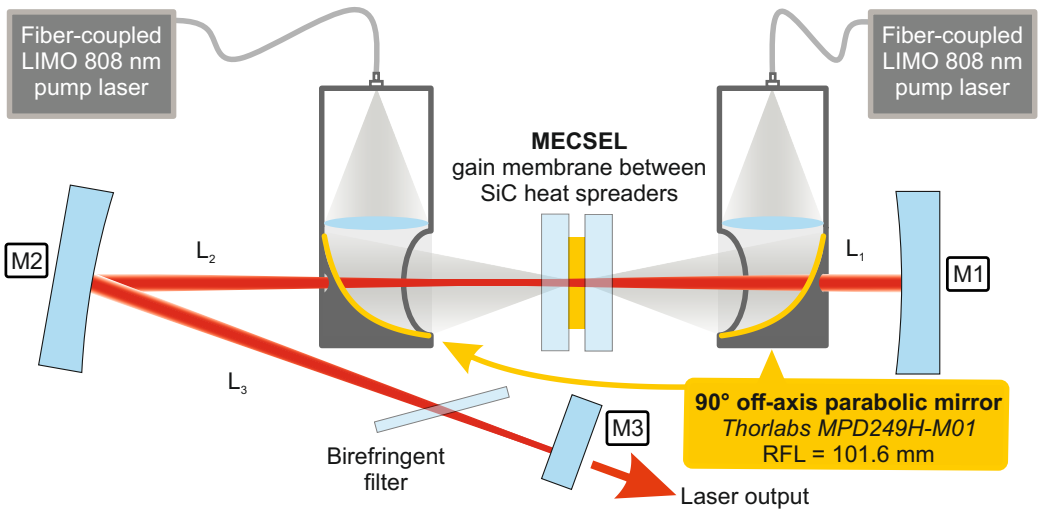

Figure 4. Experimental setup of the MECSEL employing the broadband gain structure and a V-cavity. By using 90° off-axis parabolic mirrors with a high-reflection protected gold coating, the pump beam is focused down to a nearly circular pump spot onto the laser-active membrane as illustrated.

water/glycol cooled copper heat spreaders (not drawn in Fig. 4) with an aperture diameter of 1.5 mm. The opening angle of the aperture is 60° to provide enough space for the incident pump laser.

3.2 Power transfer and spectral shift

In order to determine the power performance of the broadband MECSEL, power transfer measurements were performed. The setup configuration for these measurements was the same as depicted in Fig. 4. No birefringent filter or any other optical intra cavity element was used for the power transfer measurements, the laser resonator was operating free. The pump power was increased symmetrically and spectra were recorded for all pump power configurations. Figure 5a shows the plotted data of the power transfer measurement. Due to the relatively high

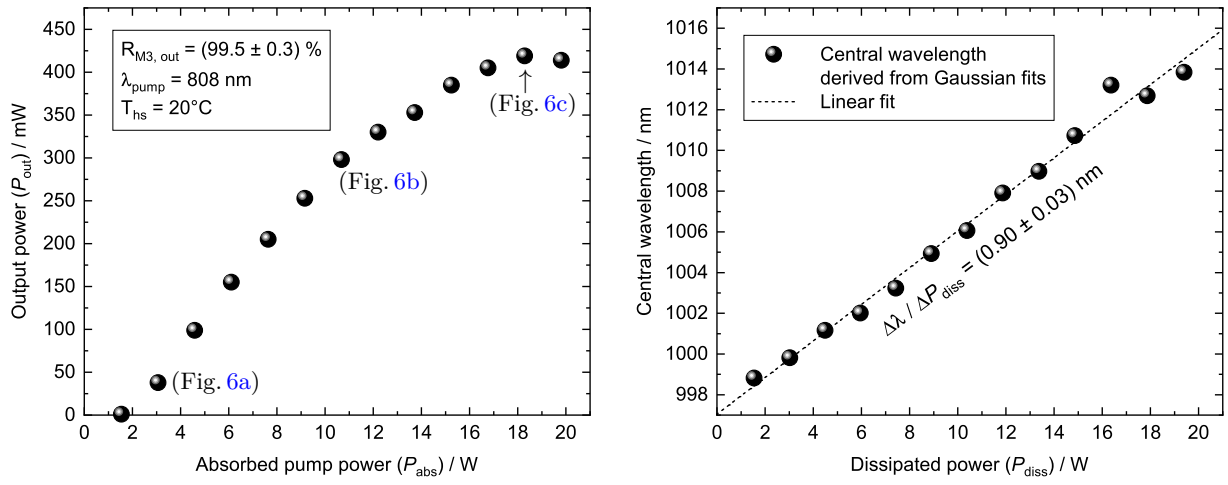

Figure 5. (a) MECSEL output power plotted over absorbed pump power. (b) The power depending spectral shift plotted here was determined during the power transfer measurement plotted in Fig. 5a.

reflectivity of the used outcoupler of $R_{\mathrm{M3,\,out}} = (99.5 \pm 0.3)\,\%$ high power emission was not expected. We see a linear increase in output power starting at the threshold of $P_{\mathrm{th}} = 1.63\,\mathrm{W}$. A little kink in the linear behaviour

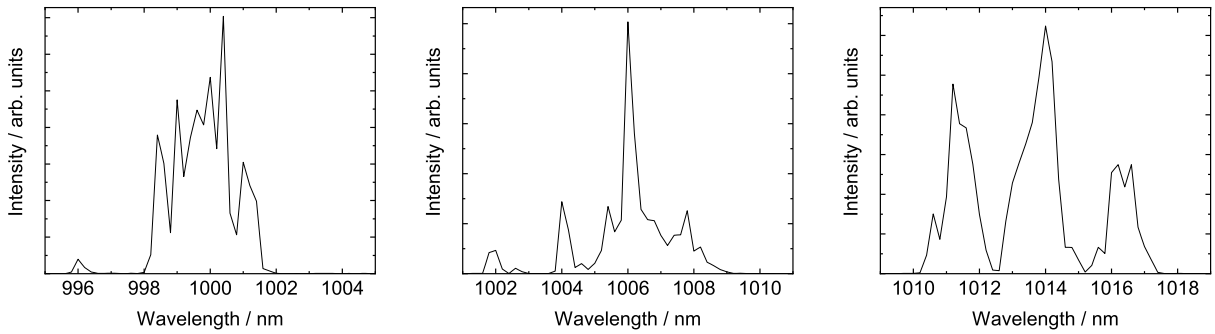

Figure 6. (a) - (c) Exemplary spectra, recorded during the power transfer measurement with indication of the power configuration in Fig. 5a.

can be seen in point (d), where also the corresponding spectrum is plotted in Fig. 6b. This might origin from a polarization jump, as no polarization maintaining element like a birefringent filter is implemented - the laser is operating freely. Besides the change in the slope efficiency, no change or deviation from the linear behaviour in the spectral shift (see Fig. 5b) is visible. More details to Fig. 5b and the use of its data can be found in Subsec. 3.3.

3.3 Thermal resistance

An essential figure of merit enabling us to determine the thermal behavior of the system is the thermal resistance R_{th}. This parameter is important for MECSELs in general as a relatively low R_{th} is one of its key benefits predicted by simulations.

Therefore, spectra were taken whilst power transfer measurements were performed, determining the spectral shift per change of dissipated power $\Delta\lambda/\Delta P_{\mathrm{diss}}$. These data are plotted in Fig. 5b. The dissipated power P_{diss} was calculated as follows:

$$P_{\mathrm{diss}} = \underbrace{P_{\mathrm{pump}} - P_{\mathrm{refl}} - P_{\mathrm{trans}}}_{=P_{\mathrm{abs}}} - P_{\mathrm{out}} \tag{1}$$

Here, P_{pump} represents the incident pump power irradiated onto the MECSEL gain element, P_{refl} is the pump power reflected by the gain element, and P_{trans} is the non-absorbed pump power transmitted through the gain element. P_{abs} represents pump power absorbed in the gain element. To determine P_{diss} the measured output power P_{out} of the MECSEL was subtracted from the absorbed pump power P_{abs}. P_{abs} was determined by subtracting P_{trans}, which was measured separately. P_{refl} was also subtracted from the separately measured incident pump power P_{pump}. The reflected pump power P_{refl} was calculated with the FRESNEL equations to be approximately 20 % of incident pump power P_{pump} at the SiC heat spreader front surface for incident angles $< 15°$. Pump transmission measurements revealed a value of 3.9 %. With these values the absorption of incident pump power by the gain element was calculated to be 76.1 %. As it can be seen in Fig. 5b the spectral shift per dissipated pump power was determined to $\Delta\lambda/P_{\mathrm{diss}} = (0.90 \pm 0.03)\,\mathrm{nm/W}$.

Furthermore, the thermal shift of the laser emission $\Delta\lambda/\Delta T_{\mathrm{hs}}$ was measured under constant pumping of $P_{\mathrm{pump}} = 6\,\mathrm{W}$ (3 W from each side). For this measurement the heat sink temperature T_{hs} was changed gradually from 5°C to 23°C by changing the water/glycol cooling temperature. The temperature difference between chiller and heat sink was determined to be in the range of 0.1°C and is therefore negligible. The thermal wavelength shift of $\Delta\lambda/\Delta T_{\mathrm{hs}} = (0.24 \pm 0.01)\,\mathrm{nm/K}$ was determined via a linear fit to the measured data which are plotted in Fig. 7. This allows to calculate the thermal resistance R_{th} of the MECSEL gain element including error propagation as follows[37]:

$$R_{\mathrm{th}} = \frac{\Delta\lambda/\Delta P_{\mathrm{diss}}}{\Delta\lambda/\Delta T_{\mathrm{hs}}} = \underline{\underline{(3.75 \pm 0.28)\,\mathrm{K/W}}} \tag{2}$$

This value is of the same order of magnitude as previously published results[22,32] with SiC heat spreaders of the same thickness. Although different gain membrane materials were used, comparability is given as the thermal

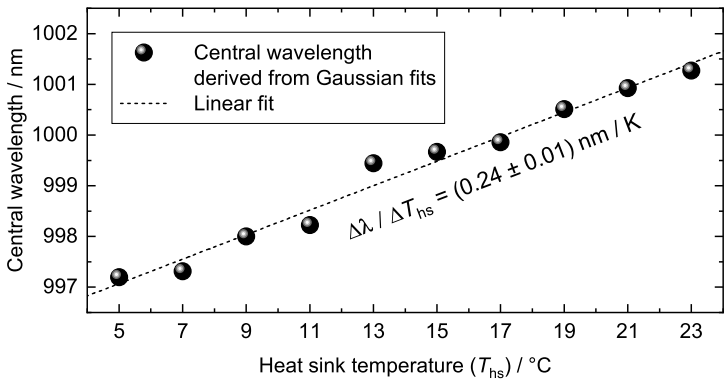

Figure 7. The heat sink temperature (T_{hs}) depending spectral shift plotted here was measured under constant incident pump power.

conductivities of the semiconductor materials are one to two orders of magnitude inferior compared to the one of SiC. The thermal conductivity of the membrane itself plays therefore a minor role.

3.4 Broadband wavelength tuning

For tuning measurements 18.0 W of incident pump power (corresponds to 13.7 W of absorbed pump power) were chosen, because beforehand experiments revealed the largest tuning range under SSP at this pump power. Higher

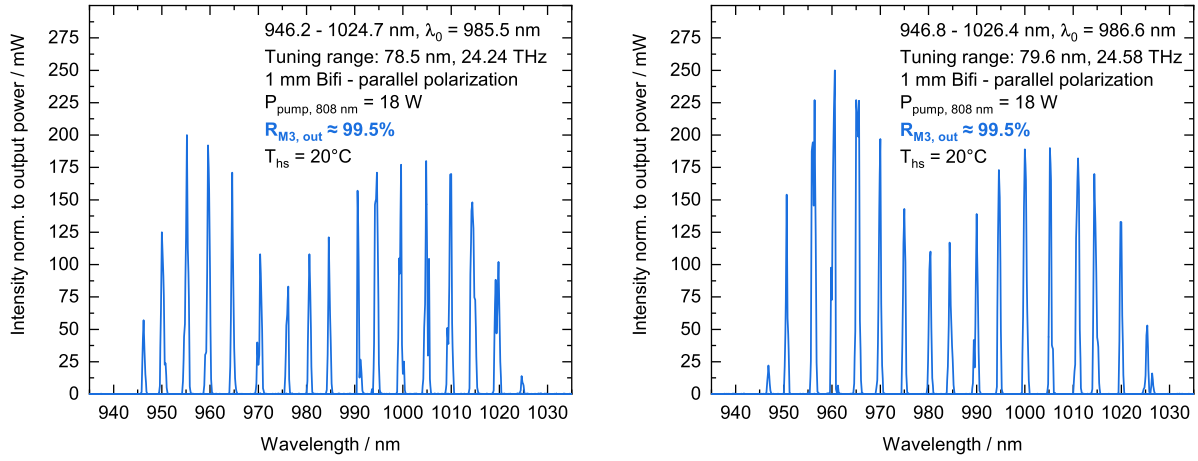

Figure 8. A set of exemplary spectra (blue curves) to depict wavelength tuning are shown in these two plots. The intensity of the spectra was normalized to the correspondingly measured output power, which was plotted over wavelength. 18 W of incident pump power were applied (a) only from the left side, and (b) only from the left right side.

pump powers lead to a smaller tuning range and worse absolute output power values due to thermal rollover under SSP condition. The spectra were recorded with an ANDO AQ-6315A™ optical spectrum analyzer with 0.05 nm resolution. The results of SSP measurements are shown in Figs. 8a and 8b. As described in Subsec. 2.1 we can see a slightly better performance for the SSP case from the right side (Fig. 8b) due to a beneficial barrier width distribution (similar to the structures described for example by Phung *et al.*[32] and Baumgärtner *et al.*[38]) for right side pumping. In the short wavelength range around 960 nm the output power is superior by even 25 %. Although this comparison was not intended, it clearly shows that the QW and barrier width distribution should be matched with the absorption behaviour of the applied pump light in future structure designs.
In order to obtain comparable data, the total incident pump power was kept the same but divided on two sides for the case of double-sided pumping. As can be seen in Fig. 9 a slightly wider tuning range of 83.1 nm or

25.55 THz was achieved compared to the single-side pumping measurements, where ∼ 79 nm were reached. The PL curve of the corresponding broadband gain structure from Fig. 3 was plotted again in Fig. 9 for comparison with the laser tuning. A further detail which can be seen in Fig. 9 is that laser emission above 100 mW was achieved in the range of from 945.0 to 1020.0 nm (75 nm). It is further noteworthy how accurately the MECSEL tuning behaviour follows the PL characteristic in a relative intensity comparison taking the spectral red shift and typical inverted parabolic shape of the corresponding QWs' gain into account.

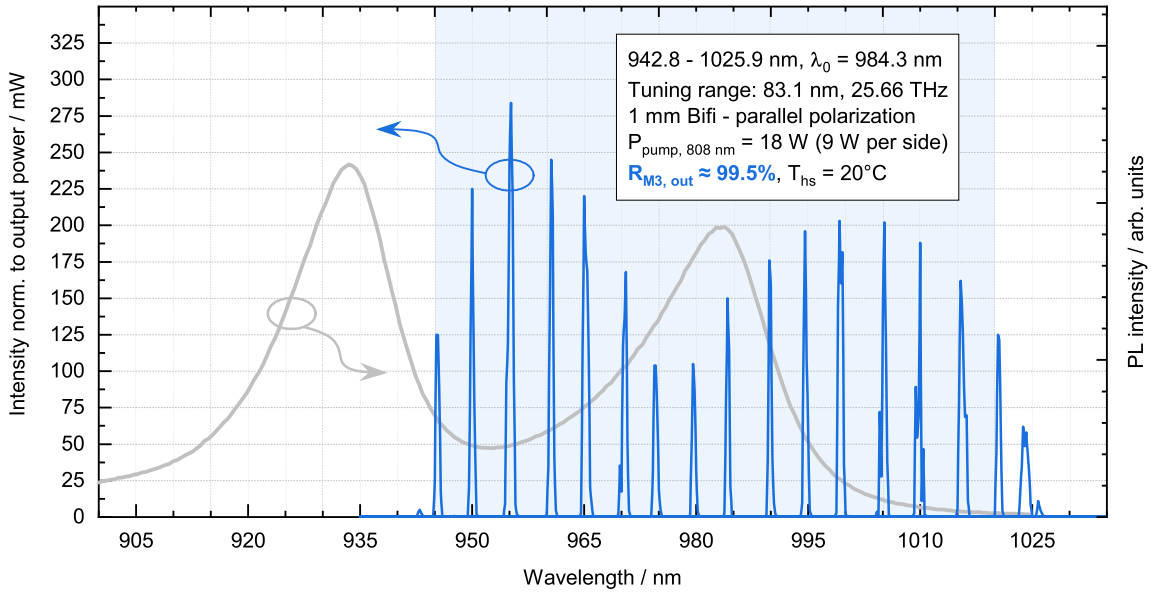

Figure 9. A set of exemplary spectra (blue curves) to depict wavelength tuning are shown in this plot. The intensity of the spectra was normalized to the correspondingly measured output power, which was plotted over wavelength. 18 W of incident pump power were applied under symmetric DSP condition. The PL (light grey curve) of the corresponding broadband gain structure from Fig. 3 was plotted here again for comparison with the tuning behaviour of the MECSEL. The light blue background indicates the tuning with powers > 100 mW.

4. CONCLUSION

The widest tuning of a vertically emitting semiconductor laser of 25.66 THz (83.1 nm) was shown. This wide tuning range from 942.8 to 1025.9 nm was reached at room temperature (20°C). The results show the tremendous capability of MECSELs utilizing multiple types of QWs for significantly increasing the tuning range of vertically emitting lasers in the future. The omission of DBRs removes the limit set by a finite stop band and allows double-side pumping, which in turn allows the usage of thicker active areas with more QW and/or QW types. The laser cavity is then built up of external dielectric mirrors, which are available with much wider stop bands to support potentially wide tuning due to the use of this variety of different QWs within the same structure. This paper also shows that exactly this concept of not to monolithically integrate DBRs but to use broadband dielectric external cavity mirrors is a valid strategy to widen the tuning ranges of excellent beam parameter (typical M^2 of MECSELs[10] is < 1.1) and high power (> 100 mW). No restrictions originating from any kind of cavity mirror were experienced during the characterization measurements as the dielectric cavity mirrors were chosen to fully cover the expected gain bandwidth and beyond.

5. OUTLOOK

In the future, it is expected to further increase the tuning range of broadband MECSELs. More different types of QWs will be implemented in the same structure. Also, different pumping wavelengths can be applied to address different QWs or barriers buried deeper within the active region. Numerical methods to optimize the gain membrane design, especially with respect to balancing the charge carrier distribution as well as taking

the different QW's gain into account, will be beneficial. To even further increase the gain or the tuning range, stacking of gain membranes will allow further improvements and flexibility.

ACKNOWLEDGMENTS

The authors would like to thank the Academy of Finland (No. 326455), the Academy of Finland PREIN Flagship Programme (No. 320165), the Horizon 2020 Marie Skłodowska-Curie Actions - NetLaS (No. 860807), the Magnus Ehrnrooth Foundation, and the Finnish Foundation for Technology Promotion for the financial support.

REFERENCES

[1] Coldren, L. A., "Monolithic Tunable Diode Lasers," *IEEE Journal of Selected Topics in Quantum Electronics* **6**(6), 988–999 (2000).

[2] Coldren, L. A., Fish, G. A., Akulova, Y., Barton, J. S., Johansson, L., and Coldren, C. W., "Tunable semiconductor lasers: a tutorial," *Journal of Lightwave Technology* **22**(1), 193–202 (2004).

[3] Berger, J. D. and Anthon, D., "Tunable MEMS devices for optical networks," *Optics and Photonics News* **14**(3), 42–49 (2003).

[4] Wieman, C. E. and Hollberg, L., "Using diode lasers for atomic physics," *Review of scientific instruments* **62**(1), 1–20 (1991).

[5] Chenais, S., Druon, F., Balembois, F., Georges, P., Gaume, R., Haumesser, P., Viana, B., Aka, G., and Vivien, D., "Spectroscopy and efficient laser action from diode pumping of a new broadly tunable crystal: Yb^{3+}:$Sr_3Y(BO_3)_3$," *Journal of the Optical Society of America B* **19**(5), 1083–1091 (2002).

[6] Bertinetto, F., Pascu, M.-L., Greco, M. A., and Bisi, M., "Studies on tunable lasers as sources for spectroscopy measurements," in [*ROMOPTO'94: Fourth Conference in Optics*], Vlad, V. I., ed., **2461**, 317–324, International Society for Optics and Photonics (1995).

[7] Jetter, M. and Michler, P., eds., [*Vertical External Cavity Surface Emitting Lasers: VECSEL Technology and Applications*], Wiley-VCH GmbH, 1st ed. (2021).

[8] Guina, M., Rantamäki, A., and Härkönen, A., "Optically pumped VECSELs: review of technology and progress," *J. Phys. D: Appl. Phys.* **50**(38), 383001 (2017).

[9] Yang, Z., Albrecht, A. R., Cederberg, J. G., and Sheik-Bahae, M., "Optically pumped DBR-free semiconductor disk lasers," *Optics Express* **23**(26), 33164–33169 (2015).

[10] Kahle, H., Mateo, C. M. N., Brauch, U., Tatar-Mathes, P., Bek, R., Jetter, M., Graf, T., and Michler, P., "Semiconductor membrane external-cavity surface-emitting laser (MECSEL)," *Optica* **3**(12), 1506–1512 (2016).

[11] Garnache, A., Kachanov, A. A., Stoeckel, F., and Planel, R., "High-sensitivity intracavity laser absorption spectroscopy with vertical-external-cavity surface-emitting semiconductor lasers," *Optics Letters* **24**(12), 826 (1999).

[12] Fan, L., Fallahi, M., Zakharian, A. R., Hader, J., Moloney, J. V., Bedford, R., Murray, J. T., Stolz, W., and Koch, S. W., "Extended tunability in a two-chip VECSEL," *IEEE Photonics Technology Letters* **19**(8), 544–546 (2007).

[13] Borgentun, C., Bengtsson, J., Larsson, A., Demaria, F., Hein, A., and Unger, P., "Optimization of a Broadband Gain Element for a Widely Tunable High-Power Semiconductor Disk Laser," *IEEE Photonics Technology Letters* **22**(13), 978–980 (2010).

[14] Paajaste, J., Suomalainen, S., Koskinen, R., Härkönen, A., Guina, M., and Pessa, M., "High-power and broadly tunable GaSb-based optically pumped VECSELs emitting near 2 µm," *Journal of Crystal Growth* **311**(7), 1917–1919 (2009).

[15] Huo, Y., Cho, C. Y., Huang, K. F., Chen, Y. F., and Lee, C. C., "Exploring the DBR superlattice effect on the thermal performance of a VECSEL with the finite element method," *Optics Letters* **44**, 327–330 (Jan 2019).

[16] Zhang, P., Zhu, R., Jiang, M., Song, Y., Zhang, D., and Cui, Y., "Size effect caused significant reduction of thermal conductivity of GaAs/AlAs distributed Bragg reflector used in semiconductor disk laser," *Optics & Laser Technology* **96**, 259 – 264 (2017).

[17] Piprek, J., Tröger, T., Schröter, B., Kolodzey, J., and Ih, C. S., "Thermal conductivity reduction in GaAs-AlAs distributed Bragg reflectors," *IEEE Photonics Technology Letters* **10**(1), 81–83 (1998).

[18] Kahle, H., Penttinen, J.-P., Phung, H.-M., Rajala, P., Tukiainen, A., Ranta, S., and Guina, M., "Comparison of single-side and double-side pumping of membrane external-cavity surface-emitting lasers," *Optics Letters* **44**(5), 1146–1149 (2019).

[19] Tatar-Mathes, P., Kahle, H., Mateo, C. M. N., Brauch, U., Bek, R., Jetter, M., Graf, T., and Michler, P., "Improved gain chip holder design for high efficient, high power AlGaInP-VECSEL," *Proc. SPIE* **10087**, 10087–10087–1 (2017).

[20] Schlosser, P. J., Hastie, J. E., Calvez, S., Krysa, A. B., and Dawson, M. D., "InP/AlGaInP quantum dot semiconductor disk lasers for CW TEM_{00} emission at 716 - 755 nm," *Optics Express* **17**(24), 21782–21787 (2009).

[21] Kahle, H., Nechay, K., Penttinen, J.-P., Tukiainen, A., Ranta, S., and Guina, M., "AlGaAs-based vertical-external-cavity surface-emitting laser exceeding 4 W of direct emission power in the 740 - 790 nm spectral range," *Optics Letters* **43**(7), 1578–1581 (2018).

[22] Phung, H.-M., Kahle, H., Penttinen, J.-P., Rajala, P., Ranta, S., and Guina, M., "Power scaling and thermal lensing in 825 nm emitting membrane external-cavity surface-emitting lasers," *Optics Letters* **45**(2), 547–550 (2020).

[23] Hastie, J. E., Hopkins, J.-M., Calvez, S., Jeon, C. W., Burns, D., Abram, R., Riis, E., Ferguson, A. I., and Dawson, M. D., "0.5-W single transverse-mode operation of an 850-nm diode-pumped surface-emitting semiconductor laser," *IEEE Photonics Technology Letters* **15**(7), 894–896 (2003).

[24] Mao, L., Zhang, X., Zhu, R., Wang, T., Wang, L., and Zhang, P., "Widely tunable external-cavity surface-emitting laser using various methods," *Applied Optics* **60**(22), 6706–6712 (2021).

[25] Broda, A., Wójcik-Jedlińska, A., Sankowska, I., Wasiak, M., Wieckowska, M., and Muszalski, J., "A 95-nm-wide Tunable Two-Mode Vertical External Cavity Surface-Emitting Laser," *IEEE Photonics Technology Letters* **29**(24), 2215–2218 (2017).

[26] Borgentun, C., Hessenius, C., Bengtsson, J., Fallahi, M., and Larsson, A., "Widely Tunable High-Power Semiconductor Disk Laser With Nonresonant AR-Assisted Gain Element on Diamond Heat Spreader," *IEEE Photonics Journal* **3**(5), 946–953 (2011).

[27] Mirkhanov, S., Quarterman, A. H., Kahle, H., Bek, R., Pecoroni, R., Smyth, C. J. C., Vollmer, S., Swift, S., Michler, P., Jetter, M., and Wilcox, K. G., "DBR-free semiconductor disc laser on SiC heatspreader emitting 10.1 W at 1007 nm," *Electronics Letters* **53**(23), 1537–1539 (2017).

[28] Yang, Z., Albrecht, A. R., Cederberg, J. G., and Sheik-Bahae, M., "80 nm tunable DBR-free semiconductor disk laser," *Applied Physics Letters* **109**(2) (2016).

[29] Butkus, M., Rautiainen, J., Okhotnikov, O. G., Hamilton, C. J., Malcolm, G. P. A., Mikhrin, S. S., Krestnikov, I. L., Livshits, D. A., and Rafailov, E. U., "Quantum Dot Based Semiconductor Disk Lasers for 1 - 1.3 µm," *IEEE Journal of Selected Topics in Quantum Electronics* **17**(6), 1763–1771 (2011).

[30] Priante, D., Zhang, M., Albrecht, A. R., Bek, R., Zimmer, M., Nguyen, C. L., Follman, D. P., Cole, G. D., and Sheik-Bahae, M., "In-Well Pumping of a Membrane External-Cavity Surface-Emitting Laser," *IEEE Journal of Selected Topics in Quantum Electronics* **28**(1), 1–7 (2022).

[31] Saarinen, E. J., Lyytikäinen, J., Ranta, S., Rantamäki, A., Sirbu, A., Iakovlev, V., Kapon, E., and Okhotnikov, O. G., "750 nm 1.5 W frequency-doubled semiconductor disk laser with a 44 nm tuning range," *Optics Lettters* **40**(19), 4380–4383 (2015).

[32] Phung, H.-M., Tatar-Mathes, P., Paranthoën, C., Levallois, C., Chevalier, N., Perrin, M., Kerchaoui, A., Kahle, H., Alouini, M., and Guina, M., "Quantum dot membrane external-cavity surface-emitting laser at 1.5 µm," *Applied Physics Letters* **118**(23), 231101 (2021).

[33] Jeżewski, B., Broda, A., Sankowska, I., Kuźmicz, A., Gołaszewska-Malec, K., Czuba, K., and Muszalski, J., "Membrane external-cavity surface-emitting laser emitting at 1640 nm," *Optics Letters* **45**(2), 539–542 (2020).

[34] Leinonen, T., Morozov, Y. A., Härkönen, A., and Pessa, M., "Vertical External-Cavity Surface-Emitting Laser for Dual-Wavelength Generation," *IEEE Photonics Technology Letters* **17**(12), 2508–2510 (2005).

[35] Phung, H.-M., Tatar-Mathes, P., Rogers, A., Rajala, P., Ranta, S., Kahle, H., and Guina, M., "Thermal behaviour and power scaling potential of membrane external-cavity surface-emitting lasers (MECSELs)," *IEEE Journal of Quantum Electronics* **XX**(XX), XXX–XXX (2022).

[36] Laurain, A., Hader, J., and Moloney, J. V., "Modeling and optimization of transverse modes in vertical-external-cavity surface-emitting lasers," *Journal of the Optical Society of America B* **36**(4), 847–854 (2019).

[37] Heinen, B., Zhang, F., Sparenberg, M., Kunert, B., Koch, M., and Stolz, W., "On the Measurement of the Thermal Resistance of Vertical-External-Cavity Surface-Emitting Lasers (VECSELs)," *IEEE Journal of Quantum Electronics* **48**(7), 934–940 (2012).

[38] Baumgärtner, S., Kahle, H., Bek, R., Schwarzbäck, T., Jetter, M., and Michler, P., "Comparison of AlGaInP-VECSEL gain structures," *Journal of Crystal Growth* **414**, 219–222 (2015). Proceedings of the Seventeenth International Conference on Metalorganic Vapor Phase Epitaxy.